J. Meas. Sci. Instrum., 2024, 15(4): 466-476. http://jmsi.publish.founderss.cn
DOI: 10.62756/jmsi.1674-8042.2024047 jmsi@nuc.edu.cn

Hypergraph regularized multi-view subspace clustering with dual tensor log-determinant

HU Keyin[1,2], LI Ting[1,2], GE Hongwei[1,2*]

1. School of Artificial Intelligence and Computer Science, Jiangnan University, Wuxi 214122, China;
2. Engineering Research Center of Intelligent Technology for Healthcare, Ministry of Education, Jiangnan University, Wuxi 214122, China

***Corresponding author:** GE Hongwei (ghw8601@163.com)

Received: March 06, 2024 **Revised:** April 30, 2024 **Accepted:** June 12, 2024

Abstract: The existing multi-view subspace clustering algorithms based on tensor singular value decomposition (t-SVD) predominantly utilize tensor nuclear norm to explore the intra view correlation between views of the same samples, while neglecting the correlation among the samples within different views. Moreover, the tensor nuclear norm is not fully considered as a convex approximation of the tensor rank function. Treating different singular values equally may result in suboptimal tensor representation. A hypergraph regularized multi-view subspace clustering algorithm with dual tensor log-determinant (HRMSC-DTL) was proposed. The algorithm used subspace learning in each view to learn a specific set of affinity matrices, and introduced a non-convex tensor log-determinant function to replace the tensor nuclear norm to better improve global low-rankness. It also introduced hyper-Laplacian regularization to preserve the local geometric structure embedded in the high-dimensional space. Furthermore, it rotated the original tensor and incorporated a dual tensor mechanism to fully exploit the intra view correlation of the original tensor and the inter view correlation of the rotated tensor. At the same time, an alternating direction of multipliers method (ADMM) was also designed to solve non-convex optimization model. Experimental evaluations on seven widely used datasets, along with comparisons to several state-of-the-art algorithms, demonstrated the superiority and effectiveness of the HRMSC-DTL algorithm in terms of clustering performance.

Key words: multi-view clustering; tensor log-determinant function; subspace learning; hypergraph regularization

0 Introduction

Clustering is a typical unsupervised data analysis method in the fields of pattern recognition and machine learning. Various clustering methods have been proposed, such as classic hierarchical clustering methods[1], density-based clustering methods[2], partition-based clustering methods[3], and subspace-based clustering methods. Now with the continuous development of internet hardware and software technologies, available data across various industries have shown an explosive growth trend. Additionally, the constant improvements in data collection methods and information technology have led to these data becoming increasingly multi-sourced. For example, images in multimedia retrieval can be described by color, texture, and edges[4]. These different features can be regarded as a specific view. At this time, the information provided by a single view is very limited. By combining multiple views for data analysis, more comprehensive information can be obtained, which has led to the emergence of multi-view learning.

To address the limitations of the aforementioned single-view clustering methods, several multi-view clustering algorithms have been proposed[5-11]. These algorithms can be roughly categorized into five types based on their mechanisms and principles[12]: collaborative training-based methods, multi-kernel learning methods, multi-view graph clustering methods, multi-view subspace clustering methods, and multi-task multi-view clustering methods. Multi-view subspace clustering methods have attracted widespread attention due to their ability to effectively explore the subspace structure of multi-view data. Their success primarily stems from two important principles[13]: the consensus principle and the complementary principle. Many multi-view subspace clustering algorithms have been proposed based on either the consensus principle, the complementary principle, or a combination of both. Most of them originate from self-representation properties, such

as sparse subspace clustering (SSC) [14] and low-rank representation (LRR) [15], which has made significant contributions to the development of subspace clustering. Furthermore, some methods utilize the consistency principle for clustering. For instance, BRBIĆ et al. [16] introduced balanced consistency objectives among different views while encouraging sparsity and low-rankness of the solution, thus constructing a shared affinity matrix across all views to learn joint subspace representations. Tang et al.[17] weighted the consistency term within the multi-view subspace clustering model, automatically assigning reasonable weight values to each view during clustering, resulting in more appropriate consistency terms. On the other hand, diversity-based methods focused more on the complementary principle. Cao et al.[18] used the hilbert-schmidt independence criterion (HSIC) to maximize the diversity of representations from different views, albeit lacking exploration of consistency.

In addition, emerging strategies based on tensor singular value decomposition with tensor nuclear norms have been developed to explore the spatial structure and higher-order information of input multi-view data. Zhang et al. [19] proposed the first tensor-based multi-view clustering method to explore complementary information from multi-view data. Wu et al.[20] constructed a tensor based on the transition probability matrix of multi-view Markov chains and utilized tensor nuclear norm based on tensor singular value decomposition to capture primary information from multiple views. Xie et al.[21] proposed a tensor multi-rank minimization clustering model with unified multi-view self-representation, which used tensor nuclear norm regularization in a unified tensor space to ensure global consistency between different views. Unfortunately, despite the considerable success of these methods, most of them aimed to study pairwise correlations between a common representation or views, assuming that the heterogeneous features of the data typically reside within the union of multiple linear subspaces, which may lead to suboptimal clustering performance. These methods didn't fully leverage the within-sample view correlations and consider using the same parameter for shrinking all singular values with tensor nuclear norm regularization, resulting in suboptimal solutions.

To address the aforementioned issues, hypergraph regularized multi-view subspace clustering with dual tensor log-determinant (HRMSC-DTL) was proposed. Specifically, a tensor-based model was adopted to learn the low-rank representation of each view. To capture high-order correlations within and between views, both tensor rotation and non-rotation were considered, and improvements were made to the tensor nuclear norm. In the tensor space, a tensor logarithmic determinant function was employed to better enhance the global low-rankness. Additionally, hypergraph regularization was employed to capture consistent manifold information hidden in multi-view data. Finally, the above analyses were integrated into a unified framework for learning. Experimental results demonstrated the superiority and effectiveness of the HRMSC-DTL algorithm in clustering performance.

1 Related work

1.1 Notations and preliminaries

Uppercase letters (e. g., $\boldsymbol{A}$) are used to denote matrices, and lowercase letters (e. g., $\boldsymbol{a}$) are used to denote vectors. For a matrice $\boldsymbol{A}\in\mathbf{R}^{n_1\times n_2\times n_3}$, it is commonly referred to as a third-order tensor, where $\boldsymbol{A}(i,:,:)$, $\boldsymbol{A}(:,i,:)$, and $\boldsymbol{A}(:,:,i)$ represent the ith horizontal, lateral, and frontal slices, respectively. And the frontal slices can also be expressed as $\boldsymbol{A}^{(i)}$. In addition, there are some related tensor operations such as the fast fourier transform (FFT) of tensor $\boldsymbol{A}$, denoted as $\boldsymbol{A}_f=fft(\boldsymbol{A},[\,],3)$, and its corresponding inverse fourier transform (IFFT) denoted as $\boldsymbol{A}=ifft(\boldsymbol{A}_f,[\,],3)$.

Definition 1 (t-SVD[22]) Given a tensor $\boldsymbol{A}\in\mathbf{R}^{n_1\times n_2\times n_3}$, then the tensor singular value decomposition (t-SVD) of $\boldsymbol{A}$ is given by

$$\boldsymbol{A}=\boldsymbol{U}\times\boldsymbol{S}\times\boldsymbol{V}^{\mathrm{T}}, \tag{1}$$

where $\boldsymbol{U}\in\mathbf{R}^{n_1\times n_1\times n_3}$ and $\boldsymbol{V}\in\mathbf{R}^{n_2\times n_2\times n_3}$ are orthogonal tensors, and $\boldsymbol{S}\in\mathbf{R}^{n_1\times n_2\times n_3}$ is a diagonal tensor.

Definition 2 (TNN[23]) Given a tensor $\boldsymbol{A}\in\mathbf{R}^{n_1\times n_2\times n_3}$, let $h=\min(n_1,n_2)$, then the tensor nuclear norm (TNN) of $\boldsymbol{A}$ is defined as

$$\|\boldsymbol{A}\|_*=\frac{1}{n_3}\sum_{k=1}^{n_3}\|\boldsymbol{A}_f^{(k)}\|_*=\frac{1}{n_3}\sum_{k=1}^{n_3}\sum_{i=1}^{h}\boldsymbol{S}_f^{(k)}(i,i). \tag{2}$$

1.2 Hypergraph

Mainfold regularization refers to hypergraph regularization, given a hypergraph $G=(V,E)$, where V denotes the vertex set, E denotes the hyperedge set, and the incidence matrix $\boldsymbol{H}\in\mathbf{R}^{|V|\times|E|}$represents the relationship between the vertex set and the hyperedge set. The normalized Laplacian matrix of the hypergraph G can be computed as

$$\boldsymbol{L}_H=\boldsymbol{D}_{\mathrm{v}}-\boldsymbol{H}\boldsymbol{W}_{\mathrm{e}}\boldsymbol{D}_{\mathrm{e}}^{-1}\boldsymbol{H}^{\mathrm{T}}, \tag{3}$$

where $\boldsymbol{D}_{\mathrm{v}}$, $\boldsymbol{D}_{\mathrm{e}}$, and $\boldsymbol{W}_{\mathrm{e}}$ respectively represent the vertex degree, hyperedge degree, and hyperedge weight. Hypergraph Laplacian regularization is based on a common manifold assumption. If two data points $\boldsymbol{x}_i$ and $\boldsymbol{x}_j$ are close

in the intrinsic geometric structure of the data distribution, then the two points will also be close in the new representation space, and neighboring points are linearly correlated. The hypergraph Laplacian regularization operator can be expressed by[24]

$$\min_{\boldsymbol{Z}^{(v)}} tr(\boldsymbol{Z}^{(v)}\boldsymbol{L}_h^{(v)}\boldsymbol{Z}^{(v)^{\mathrm{T}}}), \tag{4}$$

where $\boldsymbol{Z}^{(v)}$ and $\boldsymbol{L}_h^{(v)}$ are respectively the self-representation matrix and hypergraph Laplacian matrix of the vth view.

1.3 Tensor logarithmic determinant

In the LRR method, to recover a low-rank matrix $\boldsymbol{X}_0$ from a given observation matrix corrupted by errors $\boldsymbol{E}_0$ ($\boldsymbol{X}=\boldsymbol{X}_0+\boldsymbol{E}_0$), the regularized low-rank minimization problem can be considered as[15]

$$\min_{\boldsymbol{D},\boldsymbol{E}} rank(\boldsymbol{D})+\lambda\|\boldsymbol{E}\|_l,\ \text{s.t.}\ \boldsymbol{X}=\boldsymbol{D}+\boldsymbol{E}, \tag{5}$$

where the minimum value of $\boldsymbol{D}$ obtained from the minimization in Eq. (5) provides the low-rank recovery of the original data $\boldsymbol{X}_0$. However, minimizing the rank of a matrix in Eq. (5) is NP-hard. Therefore, a widely used convex relaxation approach is to replace the rank function with the nuclear norm. The nuclear norm technique has been proven to be an effective low-rank solution for the rank function. However, the nuclear norm approximates the rank function by linearly summing all singular values, making it a loose and biased substitute for the rank function. To overcome this drawback of the nuclear norm, Zhao et al.[25] introduced a new logarithmic determinant function to better approximate the rank function. Unlike the linear penalty function used by the nuclear norm, the new function employs a non-linear concave penalty function to regularize singular values. For a matrix $\boldsymbol{A}\in\mathbf{R}^{n\times n}$, the logarithmic determinant function is defined as

$$F(\boldsymbol{A})=\ln\det(\boldsymbol{I}+\boldsymbol{A}^{\mathrm{T}}\boldsymbol{A})=\sum_{i=1}^{n}\ln(1+\sigma_i^2(\boldsymbol{A})), \tag{6}$$

where $\sigma_i(\boldsymbol{A})$ represents the ith largest singular value of the matrix $\boldsymbol{A}$. It can be seen that unlike the linear penalty function $f(\boldsymbol{x})=\boldsymbol{x}$ used by the nuclear norm, the logarithmic determinant function $f(\boldsymbol{x})=\ln(1+\boldsymbol{x})$ employs a non-linear concave penalty function to regularize the singular values. Compared to the convex nuclear norm, the non-convex logarithmic determinant function has some superior properties. It better approximates the rank function especially for large and near-zero singular values. Therefore, compared to the nuclear norm, the logarithmic determinant function serves as a more stringent and unbiased substitute for the rank function, enabling superior low-rank tensor recovery.

Eq. (6) is extended to the form of a third-order tensor[26], defined as

$$\Psi(\boldsymbol{A})=\|\boldsymbol{A}\|_{\mathrm{TLD}}=\frac{1}{n_3}\sum_{i=1}^{\min(n_1,n_2)}\sum_{k=1}^{n_3}\ln\left|1+\boldsymbol{S}_f^2(i,i,k)\right|. \tag{7}$$

2 Proposed model

2.1 Algorithm model

Tensor-based multi-view clustering methods aim to find a tight relaxation of tensor rank to achieve the same objective. Lu et al.[23] proposed that the tensor nuclear norm based on tensor singular value decomposition (t-SVD) was the tightest convex relaxation for tensor multi-rank[27], which could provide accurate low-rank recovery. Xie et al.[21] introduced a multi-view subspace clustering method based on t-SVD (t-SVD-MSC), which employed the tensor nuclear norm based on t-SVD to constrain the rotated tensor, effectively capturing the high-order information embedded in multi-view data. And t-SVD-MSC model can be formulated as

$$\begin{aligned}&\min_{\boldsymbol{A}^{(v)},\boldsymbol{E}^{(v)}}\lambda\|\boldsymbol{E}\|_{2,1}+\|\boldsymbol{A}\|_*,\\ &\text{s.t.}\ \boldsymbol{X}^{(v)}=\boldsymbol{X}^{(v)}\boldsymbol{A}^{(v)}+\boldsymbol{E}^{(v)},v=1,\cdots,V,\\ &\boldsymbol{A}=\Phi(\boldsymbol{A}^{(1)},\boldsymbol{A}^{(2)},\cdots,\boldsymbol{A}^{(V)}),\\ &\boldsymbol{E}=[\boldsymbol{E}^{(1)};\boldsymbol{E}^{(2)};\cdots;\boldsymbol{E}^{(V)}].\end{aligned} \tag{8}$$

Although the method (8) considers the intra-view high-order correlations in the tensor space and achieves decent performance, it overlooks the inter-view high-order correlations. To address this limitation, a dual tensor mechanism was introduced, and an additional term $\tilde{\boldsymbol{A}}=\Phi(\boldsymbol{A})$ was introduced to rotate the original tensor $\boldsymbol{A}$. To leverage the intra-view correlations among samples within each view, the affinity graphs $\boldsymbol{A}^{(v)}$ are stacked into a tensor $\boldsymbol{A}\in\mathbf{R}^{n\times n\times V}$. To utilize the inter-view correlations within different samples, the tensor $\boldsymbol{A}$ is rotated into a tensor $\tilde{\boldsymbol{A}}\in\mathbf{R}^{n\times V\times n}$. Additionally, hypergraph-induced hyper Laplacian regularization can effectively preserve the local geometric structure embedded in high-dimensional space. And the analysis in section 1.3 showed that tensor log-determinant had better properties compared to tensor nuclear norm. Inspired by this, the paper considered using tensor log-determinant for recovering low-rank tensor representations in multi-view subspace clustering, rather than solely relying on tensor nuclear norm. In a word, the HRMSC-DTL method was based t-SVD-MSC model and incorporated the dual tensor mechanism, hypergraph regularization, and tensor log-determinant function. Then, after integrating the above three parts into a unified framework, the final proposed

HRMSC-DTL model can be represented as

$$\begin{aligned}&\min_{\boldsymbol{A}^{(v)},\boldsymbol{E}^{(v)}}\|\boldsymbol{A}\|_{\mathrm{TLD}}+\alpha\|\tilde{\boldsymbol{A}}\|_{\mathrm{TLD}}+\lambda_1\|\boldsymbol{E}\|_{2,1}+\\&\lambda_2\sum_{v=1}^{V}tr(\boldsymbol{A}^{(v)}\boldsymbol{L}_h^{(v)}\boldsymbol{A}^{(v)\mathrm{T}}),\\&\text{s.t. }\boldsymbol{X}^{(v)}=\boldsymbol{X}^{(v)}\boldsymbol{A}^{(v)}+\boldsymbol{E}^{(v)},v=1,\cdots,V,\\&\boldsymbol{A}=\Phi(\boldsymbol{A}^{(1)},\boldsymbol{A}^{(2)},\cdots,\boldsymbol{A}^{(V)}),\\&\boldsymbol{E}=[\boldsymbol{E}^{(1)};\boldsymbol{E}^{(2)};\cdots;\boldsymbol{E}^{(V)}].\end{aligned}\tag{9}$$

2.2 Algorithm optimization

The proposed model (9) is solved using the augmented Lagrange method (ALM) and alternating direction minimization (ADM) optimization algorithms, that is to say, updating one variable while fixing the other variables. To make the objective function (9) separable, two auxiliary tensors $\boldsymbol{P}$ and $\boldsymbol{K}$ are introduced to replace $\boldsymbol{A}$ and $\tilde{\boldsymbol{A}}$, respectively. v auxiliary variables $\boldsymbol{B}^{(v)}$ are introduced to replace $\boldsymbol{A}^{(v)}$, problem (9) is transformed into a convex optimization problem. The corresponding augmented Lagrangian function is

$$\begin{aligned}&\mathcal{L}(\boldsymbol{A}^{(v)};\boldsymbol{E}^{(v)};\boldsymbol{B}^{(v)};\boldsymbol{P};\boldsymbol{K})=\|\boldsymbol{P}\|_{\mathrm{TLD}}+\\&\alpha\|\boldsymbol{K}\|_{\mathrm{TLD}}+\lambda_1\|\boldsymbol{E}\|_{2,1}+\lambda_2\sum_{v=1}^{V}tr(\boldsymbol{B}^{(v)}\boldsymbol{L}_h^{(v)}\boldsymbol{B}^{(v)\mathrm{T}})+\\&\frac{\rho}{2}\left\|\boldsymbol{P}-\left(\boldsymbol{A}+\frac{\boldsymbol{M}_1}{\rho}\right)\right\|_{\mathrm{F}}^2+\frac{\rho}{2}\left\|\boldsymbol{K}-\left(\boldsymbol{A}+\frac{\boldsymbol{M}_2}{\rho}\right)\right\|_{\mathrm{F}}^2+\\&\sum_{v=1}^{V}\frac{\mu_1}{2}\left\|\boldsymbol{E}^{(v)}-(\boldsymbol{X}^{(v)}-\boldsymbol{X}^{(v)}\boldsymbol{A}^{(v)}+\frac{\boldsymbol{Y}_1^{(v)}}{\mu_1})\right\|_{\mathrm{F}}^2\\&+\sum_{v=1}^{V}\frac{\mu_2}{2}\left\|\boldsymbol{B}^{(v)}-\left(\boldsymbol{A}^{(v)}+\frac{\boldsymbol{Y}_2^{(v)}}{\mu_2}\right)\right\|_{\mathrm{F}}^2,\end{aligned}\tag{10}$$

where $\boldsymbol{M}_1$, $\boldsymbol{M}_2$, $\boldsymbol{Y}_1^{(v)}$, and $\boldsymbol{Y}_2^{(v)}$ are Lagrange multipliers, and μ_1, μ_2, ρ are corresponding penalty factors. Below is the detailed solving process.

$\boldsymbol{A}^{(v)}$-subproblem: By fixing $\boldsymbol{E}^{(v)}$, $\boldsymbol{B}^{(v)}$, $\boldsymbol{P}$, and $\boldsymbol{K}$, $\boldsymbol{A}^{(v)}$ can be updated by solving

$$\begin{aligned}&\min_{\boldsymbol{A}^{(v)}}\frac{\mu_1}{2}\left\|\boldsymbol{E}^{(v)}-\left(\boldsymbol{X}^{(v)}-\boldsymbol{X}^{(v)}\boldsymbol{A}^{(v)}+\frac{\boldsymbol{Y}_1^{(v)}}{\mu_1}\right)\right\|_{\mathrm{F}}^2+\\&\frac{\mu_2}{2}\left\|\boldsymbol{B}^{(v)}-\left(\boldsymbol{A}^{(v)}+\frac{\boldsymbol{Y}_2^{(v)}}{\mu_2}\right)\right\|_{\mathrm{F}}^2+\frac{\rho}{2}\left\|\boldsymbol{P}^{(v)}-\left(\boldsymbol{A}^{(v)}+\frac{\boldsymbol{M}_1^{(v)}}{\rho}\right)\right\|_{\mathrm{F}}^2\\&+\frac{\rho}{2}\left\|\boldsymbol{K}^{(v)}-\left(\boldsymbol{A}^{(v)}+\frac{\boldsymbol{M}_2^{(v)}}{\rho}\right)\right\|_{\mathrm{F}}^2.\end{aligned}\tag{11}$$

The closed-form solution can be obtained by taking the derivative of Eq. (11) and setting the derivative to zero.

$$\begin{aligned}\boldsymbol{A}^{(v)*}=&[(\mu_2+2\rho)\boldsymbol{I}+\mu_1\boldsymbol{X}^{(v)\mathrm{T}}\boldsymbol{X}^{(v)}]^{-1}\times\\&\left[\mu_1\boldsymbol{X}^{(v)\mathrm{T}}\left(\boldsymbol{X}^{(v)}-\boldsymbol{E}^{(v)}+\frac{\boldsymbol{Y}_1^{(v)}}{\mu_1}\right)\mu_2\boldsymbol{B}^{(v)}-\right.\\&\left.\boldsymbol{Y}_2^{(v)}+\rho\boldsymbol{P}^{(v)}-\boldsymbol{W}_1^{(v)}+\rho\boldsymbol{K}^{(v)}-\boldsymbol{M}_2^{(v)}\right].\end{aligned}\tag{12}$$

$\boldsymbol{E}^{(v)}$-subproblem: By fixing $\boldsymbol{A}^{(v)}$, the solution of $\boldsymbol{E}^{(v)}$ is equivalent to solving

$$\boldsymbol{E}^*=\arg\min_{\boldsymbol{E}}\frac{\lambda_1}{\mu_1}\|\boldsymbol{E}\|_{2,1}+\frac{1}{2}\|\boldsymbol{E}-\boldsymbol{D}\|_{\mathrm{F}}^2,\tag{13}$$

where $\boldsymbol{D}$ is constructed by vertically concatenating matrices $\boldsymbol{X}^{(v)}-\boldsymbol{X}^{(v)}\boldsymbol{A}^{(v)}+\boldsymbol{Y}_1^{(v)}/\mu_1$ along the columns, and the subproblem (13) is

$$\boldsymbol{E}_{:,i}^*=\begin{cases}\dfrac{\|\boldsymbol{D}_{:,i}\|_2-\dfrac{\lambda_1}{\mu_1}}{\|\boldsymbol{D}_{:,i}\|_2}\boldsymbol{D}_{:,i}, & \|\boldsymbol{D}_{:,i}\|_2\dfrac{\lambda_1}{\mu_1};\\0, & \text{otherwise.}\end{cases}\tag{14}$$

$\boldsymbol{B}^{(v)}$-subproblem: By fixing $\boldsymbol{A}^{(v)}$ and $\boldsymbol{L}_h^{(v)}$, the closed-form solution $\boldsymbol{B}^{(v)}$ can be computed as

$$\begin{aligned}&\arg\min_{\boldsymbol{B}^{(v)}}\lambda_2\sum_{v=1}^{V}tr(\boldsymbol{B}^{(v)}\boldsymbol{L}_h^{(v)}\boldsymbol{B}^{(v)\mathrm{T}})+\\&\frac{\mu_2}{2}\left\|\boldsymbol{B}^{(v)}-(\boldsymbol{A}^{(v)}+\frac{\boldsymbol{Y}_2^{(v)}}{\mu_2})\right\|_{\mathrm{F}}^2.\end{aligned}\tag{15}$$

Let the derivative of Eq. (15) be zero, then there is

$$\boldsymbol{B}^{(v)*}=(\mu_2\boldsymbol{A}^{(v)}-\boldsymbol{Y}_2^{(v)})(2\lambda_2\boldsymbol{L}_h^{(v)}+\mu_2\boldsymbol{I})^{-1}.\tag{16}$$

$\boldsymbol{P}$-subproblem: By fixing $\boldsymbol{A}^{(v)}$, solving $\boldsymbol{P}$ is equivalent to solving the subproblem (17).

$$\begin{aligned}&\arg\min_{\boldsymbol{P}}\|\boldsymbol{P}\|_{\mathrm{TLD}}+\frac{\rho}{2}\left\|\boldsymbol{P}-(\boldsymbol{A}+\frac{\boldsymbol{M}_1}{\rho})\right\|_{\mathrm{F}}^2=\\&\arg\min_{\boldsymbol{P}}\|\boldsymbol{P}\|_{\mathrm{TLD}}+\frac{1}{2\tau}\|\boldsymbol{P}-\boldsymbol{T}\|_{\mathrm{F}}^2,\end{aligned}\tag{17}$$

where $\rho=1/\tau$, $\boldsymbol{T}=\boldsymbol{A}+\tau\boldsymbol{M}_1$, then the Eq. (17) can be transformed into

$$\boldsymbol{P}_f^{(k)*}=\arg\min_{\boldsymbol{P}_f^{(k)}}\tau\|\boldsymbol{P}_f^{(k)}\|_{\mathrm{TLD}}+\frac{1}{2}\|\boldsymbol{P}_f^{(k)}-\boldsymbol{T}_f^{(k)}\|_{\mathrm{F}}^2.\tag{18}$$

Performing singular value decomposition on Eq. (18), then Eq. (18) is equivalent to solving

$$\arg\min_{\sigma_i^{(k)}}\ln(1+\sigma_i^{(k)2})+\frac{1}{2\tau}\left[\sigma_i^{(k)}-\sigma_i(\boldsymbol{T}_f^{(k)})\right]^2,\tag{19}$$

where $\sigma_i(\boldsymbol{T}_f^{(k)})$ denotes the ith largest singular value of tensor $\boldsymbol{T}_f^{(k)}$, and $\sigma_i^{(k)}$ represents the ith largest singular value of the kth frontal slice of tensor $\boldsymbol{P}$ in the Fourier domain.

$\boldsymbol{K}$-subproblem: By fixing $\boldsymbol{A}^{(v)}$, solving $\boldsymbol{K}$ is equivalent to solving

$$\arg\min_{\boldsymbol{K}}\|\boldsymbol{K}\|_{\mathrm{TLD}}+\frac{\rho}{2}\left\|\boldsymbol{K}-\left(\boldsymbol{A}+\frac{\boldsymbol{M}_2}{\rho}\right)\right\|_{\mathrm{F}}^2.\tag{20}$$

The solution to Eq. (20) is similar to that of the $\boldsymbol{P}$-subproblem in Eq. (17).

2.3 Complexity analysis

From the algorithm optimization process, it can be observed that the main computational costs of HRMSC-DTL algorithm lie in updating variables $\boldsymbol{A}^{(v)}$, $\boldsymbol{L}_h^{(v)}$, $\boldsymbol{E}^{(v)}$, $\boldsymbol{B}^{(v)}$, $\boldsymbol{P}$, and $\boldsymbol{K}$. When updating $\boldsymbol{A}^{(v)}$, the time complexity of solving the linear system is $\boldsymbol{O}(VN^3)$. The hyper-Laplacian matrix $\boldsymbol{L}_h^{(v)}$ has a time complexity of $\boldsymbol{O}(VN^2\ln(N))$. When updating $\boldsymbol{E}^{(v)}$, the time complexity will be $\boldsymbol{O}(VN\sum d_v)$. Updating $\boldsymbol{P}$ has time complexities $\boldsymbol{O}(VN^2\ln(N)+N^2V^2)$. Lastly, updating $\boldsymbol{K}$ has a time complexity of $\boldsymbol{O}(VN^2\ln(N)+VN^3)$. So the overall time complexity of the proposed algorithm per iteration is approximately $\boldsymbol{O}(VN^3)$.

3 Experiments

3.1 Datasets

To validate the effectiveness and robustness of the proposed method, experiments were conducted on seven widely used datasets. Four applications are included: 1) Face image (Yale[21], ORL[21], and Notting-Hill[28]datasets); 2) Document (BBCSport[29] dataset, Wikipedia[30]); 3) Scene image (Scene-15[21] dataset); 4) Object image (COIL-20[21] dataset). The detailed descriptions of the seven datasets are shown in Table 1.

Table 1 Introduction of different experimental datasets

Datasets	No. of samples	No. of views	No. of clusters
Yale	165	3	15
BBCSport	544	2	5
ORL	400	3	40
Notting-Hill	550	3	5
Wikipedia	693	2	10
COIL-20	1 440	3	20
Scene-15	4 485	3	15

3.2 Compared methods

For a comprehensive comparison, several state-of-the-art multi-view clustering methods were selected as competitors to compare with the proposed method.

Spectral clustering[31] applies a standard spectral clustering method to each view individually, then selects the best-performing data among multiple views, denoted as $\mathrm{SC}_{\mathrm{best}}$.

Building upon multi-view subspace clustering, CoMSC[32] (Multiview subspace clustering via co-training robust data representation) adopts a co-training robust data representation method, which jointly learns data redundancy and consistent self-representation through collaborative training.

LTMSC[19] (Low-rank tensor constrained multiview subspace clustering) explores high-order correlations of multiview features through a multiview clustering method constrained by low-rank tensors.

T-SVD-MSC[21] (On unifying multi-view self-representations for clustering by tensor multi-rank minimization) constrains rotated tensors using tensor nuclear norm to effectively represent the higher-order information embedded in multi-view data.

HLR-M^{2}VS[29] (Hyper-laplacian regularized multilinear multiview self-representations for clustering and semisupervised learning) is a tensor-based multi-view clustering method with added local geometric constraints on top of t-SVD-MSC.

SM^{2}SC[33] (Split multiplicative multi-view sub-space clustering) designs a split multiplicative model for multi-view subspace clustering, which utilizes a multiplicative decomposition scheme and variable splitting approach to extract consistent components.

HNLR[30] (Hyper-Laplacian regularized non-convex low-rank representation for multi-view subspace clustering) introduces a non-convex Laplacian function on top of HLR-M^{2}VS to replace tensor nuclear norm, thereby improving the approximation performance of global low-rank structures.

CELT[28] (Collaborative embedding learning via tensor integration for multi-view clustering) is a collaborative embedding learning via tensors, which jointly learns the intra-view affinity graphs of each view from both the original space and the low-dimensional space.

3.3 Experimental results and analysis

To accurately evaluate the performance of different clustering algorithms, this study employed six widely used evaluation metrics for comprehensive assessment, including accuracy (ACC), normalized mutual information (NMI), adjusted rand index (AR), precision, recall, and F-score. Higher values for all these evaluation metrics indicate better clustering performance. Due to the different feature scales of various datasets, the data matrices were normalized for each view. Tables 2 to 8 present detailed clustering results in terms of NMI, AR, ACC, recall, precision, and F-score obtained by different clustering methods on the seven real datasets.

To ensure the fairness of the experiments, each algorithm was run 10 times, and the results of the 10 runs were averaged as the final clustering result. In Tables 2 to 8, the best clustering results for each dataset are highlighted in bold, while the second-best results are underscored for emphasis.

Table 2 Experimental results of different methods on Yale dataset

Method	NMI	AR	ACC	Recall	Precision	*F*-score
SC_{best}	0.711	0.478	0.685	0.556	0.475	0.512
LTMSC	0.765	0.570	0.741	0.629	0.569	0.598
CoMSC	0.671	0.445	0.646	0.514	0.453	0.481
t-SVD-MSC	0.908	0.910	0.963	0.927	0.904	0.915
HLR-M^2VS	0.791	0.598	0.782	0.682	0.575	0.624
SM^2SC	0.687	0.465	0.648	0.559	0.455	0.501
HNLR	0.991	0.989	0.993	0.995	0.990	0.995
CELT	0.962	0.964	0.968	0.975	0.937	0.937
HRMSC-DTL	**1.000**	**1.000**	**1.000**	**1.000**	**1.000**	**1.000**

Table 3 Experimental results of different methods on BBCSport dataset

Method	NMI	AR	ACC	Recall	Precision	*F*-score
SC_{best}	0.703	0.571	0.699	0.892	0.571	0.696
LTMSC	0.930	0.750	0.795	0.837	0.766	0.768
CoMSC	0.857	0.885	0.956	0.908	0.917	0.912
t-SVD-MSC	0.993	0.967	0.970	0.991	0.946	0.968
HLR-M^2VS	0.989	0.993	0.997	0.993	0.997	0.995
SM^2SC	0.935	0.954	0.978	0.959	0.971	0.965
HNLR	0.995	0.997	0.999	0.997	0.999	0.998
CELT	0.993	0.997	0.998	0.997	0.998	0.997
HRMSC-DTL	**1.000**	**1.000**	**1.000**	**1.000**	**1.000**	**1.000**

Table 4 Experimental results of different methods on ORL dataset

Method	NMI	AR	ACC	Recall	Precision	*F*-score
SC_{best}	0.884	0.665	0.725	0.728	0.610	0.664
LTMSC	0.930	0.750	0.795	0.837	0.766	0.768
CoMSC	0.851	0.601	0.711	0.661	0.567	0.612
t-SVD-MSC	0.993	0.967	0.970	0.991	0.946	0.968
HLR-M^2VS	**1.000**	**1.000**	**1.000**	**1.000**	**1.000**	**1.000**
SM^2SC	0.941	0.701	0.817	0.897	0.587	0.709
HNLR	**1.000**	**1.000**	**1.000**	**1.000**	**1.000**	**1.000**
CELT	0.998	0.994	0.998	0.995	0.995	0.995
HRMSC-DTL	**1.000**	**1.000**	**1.000**	**1.000**	**1.000**	**1.000**

Table 5 Experimental results of different methods on Notting-Hill dataset

Method	NMI	AR	ACC	Recall	Precision	*F*-score
SC_{best}	0.723	0.712	0.816	0.776	0.780	0.775
LTMSC	0.779	0.777	0.868	0.814	0.830	0.825
CoMSC	0.718	0.658	0.840	0.732	0.734	0.733
t-SVD-MSC	0.900	0.900	0.957	0.907	0,937	0,922
HLR-M^2VS	0.967	0.972	0.988	0.975	0.982	0.979
SM^2SC	0.944	0.945	0.963	0.969	0.946	0.957
HNLR	0.979	0.985	0.991	0.982	0.990	0.982
CELT	0.943	0.944	0.969	0.971	0.959	0.957
HRMSC-DTL	**0.989**	**0.994**	**0.996**	**0.996**	**0.994**	**0.995**

Table 6 Experimental results of different methods on Wikipedia dataset

Method	NMI	AR	ACC	Recall	Precision	*F*-score
SC_{best}	0.477	0.413	0.518	0.458	0.465	0.456
LTMSC	0.496	0.407	0.532	0.461	0.480	0.471
CoMSC	0.534	0.437	0.581	0.485	0.494	0.491
t-SVD-MSC	0.480	0.393	0.527	0.447	0.470	0.458
HLR-M^2VS	0.513	0.417	0.577	0.475	0.485	0.480
SM^2SC	0.531	0.423	0571	0.493	0.482	0.487
HNLR	0.530	0.447	0.603	0.496	0.516	0.506
CELT	**0.553**	0.450	0.591	**0.520**	0.503	0.511
HRMSC-DTL	0.539	**0.460**	**0.610**	0.499	**0.535**	**0.517**

Table 7 Experimental results of different methods on COIL-20 dataset

Method	NMI	AR	ACC	Recall	Precision	*F*-score
SC_{best}	0.806	0.619	0.672	0.692	0.596	0.604
LTMSC	0.862	0.748	0.804	0.776	0.741	0.761
CoMSC	0.795	0.559	0.652	0.685	0.510	0.584
t-SVD-MSC	0.884	0.786	0.830	0.808	0.785	0.800
HLR-M^2VS	0.960	0.833	0.852	0.949	0.757	0.842
SM^2SC	0.975	0.922	0.920	0.958	0.896	0.926
HNLR	0.983	0.936	0.930	0.976	0.906	0.939
CELT	0.970	0.939	0.950	0.963	0.922	0.943
HRMSC-DTL	**0.987**	**0.977**	**0.988**	**0.978**	**0.978**	**0.978**

Table 8 Experimental results of different methods on Scene-15 dataset

Method	NMI	AR	ACC	Recall	Precision	*F*-score
SC_{best}	0.421	0.270	0.437	0.329	0.314	0.321
LTMSC	0.571	0.424	0.574	0.479	0.452	0.465
CoMSC	0.538	0.359	0.497	0.445	0.376	0.407
t-SVD-MSC	0.858	0.771	0.812	0.839	0.743	0.788
HLR-M^2VS	0.895	0.850	0.878	0.871	0.850	0.861
SM^2SC	0.632	0.515	0.645	0.566	0.533	0.549
HNLR	0.931	0.889	0.897	0.911	0.883	0.897
CELT	0.964	0.959	0.980	0.958	0.966	0.962
HRMSC-DTL	**0.974**	**0.971**	**0.985**	**0.970**	**0.976**	**0.979**

It can be observed that the HRMSC-DTL algorithm achieved nearly optimal clustering performance on several test datasets compared to other clustering methods. Specifically, on the Yale and BBCSport datasets, the proposed method achieved nearly perfect clustering results. On the ORL dataset, the proposed method and the HLR-M^2VS method both achieved excellent clustering results. Additionally, on the Notting-Hill and COIL-20 datasets, the proposed method achieved performance metrics of over 97%, surpassing t-SVD-MSC by approximately 9.8% and 11.6% in terms of NMI, respectively. It is noteworthy that the proposed method also performs well on the larger-scale scene-15 dataset, showing a 1.0% improvement in NMI compared to the second-best method. Overall, most multi-view clustering methods outperform SC_{best}, indicating that considering multiple views generally leaded to better performance than using a single view. Furthermore, it can be observed from Tables 2 to 8 that the HNLR method achieves second-best results on most datasets, which can be attributed to the introduction of a non-convex Laplacian function to replace the tensor nuclear norm. Additionally, the proposed method outperforms t-SVD-MSC on almost all datasets, mainly because the HRMSC-DTL algorithm simultaneously considers intra-view and inter-view correlations and employs tensor logarithmic determinant functions to approximate the tensor rank,

thus better extracting high-order information between different views of multi-view data.

3.4 Visualization analysis

To visually observe the clustering performance of the HRMSC-DTL algorithm more intuitively, t-SNE method and affinity matrices were employed for visualization analysis on the Yale and ORL datasets in this study. T-SNE method projected the original features and consistency affinity matrix of each view to a 2D space for visualization and analysis. The experimental results are shown in Fig. 1, where (a), (b), and (c) represent the t-SNE visualization of the three original view features on the Yale dataset, while (e), (f), and (g) represent the t-SNE visualization of the three original view features on the ORL dataset. (d) and (h) show the t-SNE visualization of the ideal similarity matrices obtained by the HRMSC-DTL algorithm on the Yale and ORL datasets, respectively. Different colors indicate different clustering categories. It can be observed that the HRMSC-DTL algorithm effectively achieve clustering functionality, with clusters of different colors tightly clustered together, further demonstrating the effectiveness of the proposed HRMSC-DTL algorithm in terms of clustering performance.

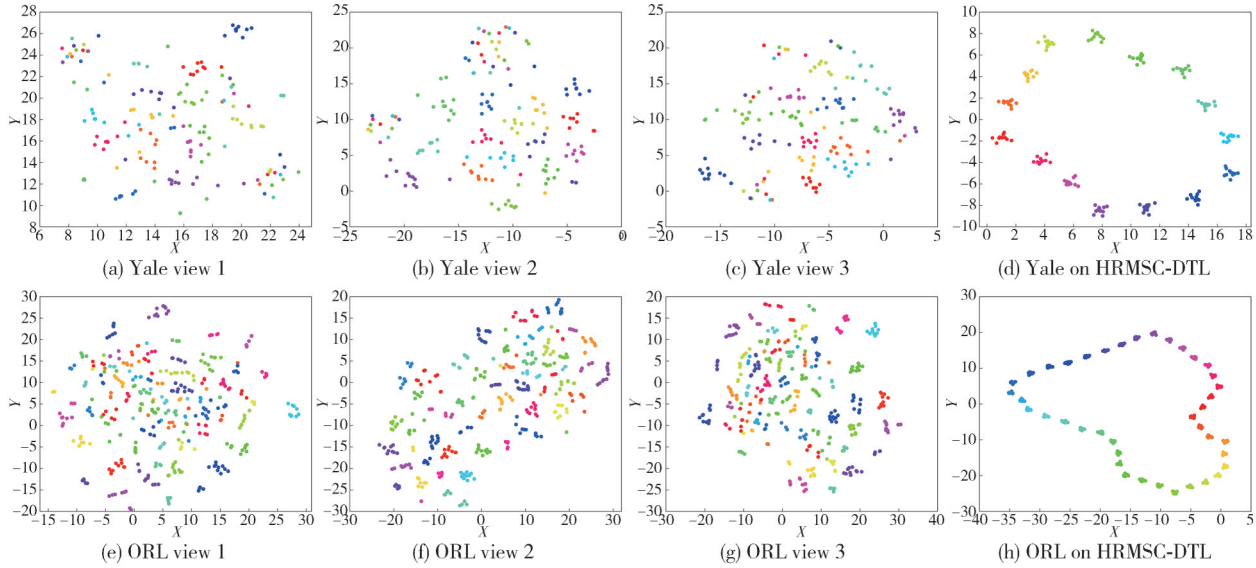

Fig. 1 Visualization results of t-SNE on Yale and ORL datasets

For the visualization of the affinity matrices as shown in Fig. 2, it can be observed that larger values tend to concentrate on the diagonal blocks. Additionally, compared to the t-SVD-MSC and HLR-M^{2}VS algorithms, the affinity matrices generated by the proposed HRMSC-DTL algorithm exhibits clearer block-diagonal structures. It implies that more discriminative matrix information can be revealed, leading to better clustering results.

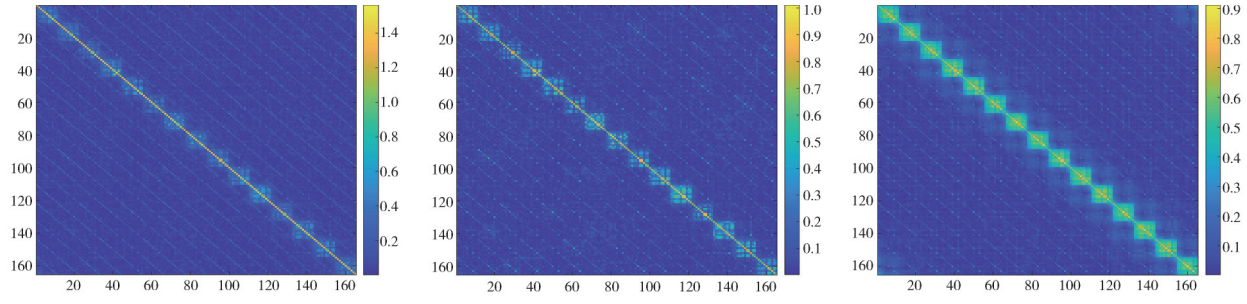

Fig. 2 Affinity matrices of three clustering methods on Yale dataset

3.5 Parameter sensitivity analysis

The HRMSC-DTL method has three free parameters, denoted as α, λ_1, and λ_2, which needs to be adjusted. Parameter analysis was conducted on two benchmark datasets to study the influence of these three parameters on the accuracy of the HRMSC-DTL algorithm. The ranges of α, λ_1, and λ_2 are set to $\{0.000\,1, 0.001, 0.01, 0.1, 1\}$. Different ranges of α, λ_1, and λ_2 were applied to the algorithm on different test datasets. The experimental results are shown in Figs. 3 to 5. In Fig. 3, when the parameter λ_2 is fixed, the algorithm demonstrates good

stability when $\alpha \in \{0.000\,1, 0.001\}$ and $\lambda_1 \in \{0.1, 1\}$. In Fig.4, when parameter λ_1 is fixed, good clustering results can be obtained with different values of α and λ_2.

However, in Fig.5(a), when α is fixed, setting both λ_1 and λ_2 to 1 leads to poor experimental performance, indicating the need for more appropriate parameter values to balance the two factors, which can potentially lead to better results.

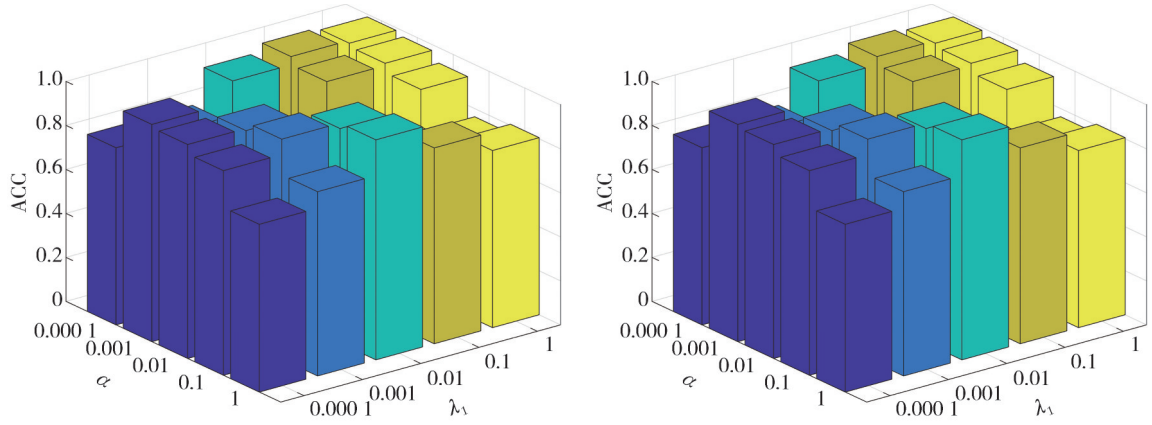

(a) Yale (b) ORL

Fig. 3 Sensitivity analysis of α and λ_1 in terms of ACC on Yale and ORL datasets

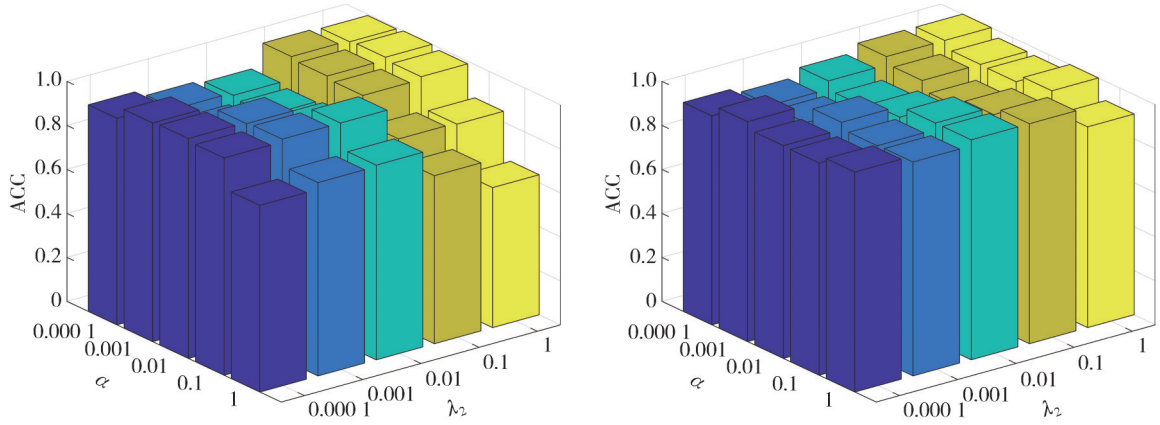

(a) Yale (b) ORL

Fig. 4 Sensitivity analysis of α and λ_2 in terms of ACC on Yale and ORL datasets

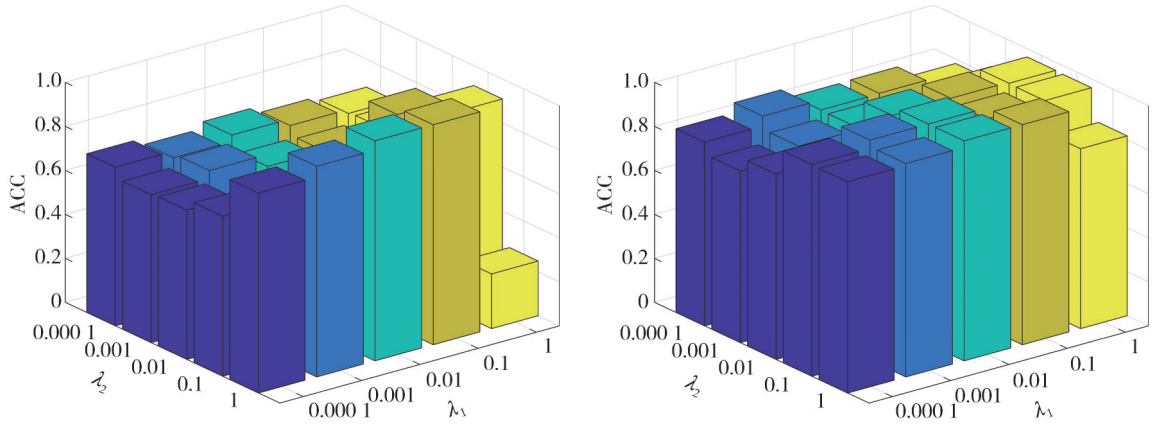

(a) Yale (b) ORL

Fig. 5 Sensitivity analysis of λ_1 and λ_2 in terms of ACC on Yale and ORL datasets

3.6 Ablation study

To further analyze the HRMSC-DTL algorithm, an ablation study was conducted to investigate the role of dual tensors mechanism, hypergraph regularization, and the strategy of replacing the tensor nuclear norm with the tensor logarithm function. It was evidenced that the clustering performance of the HRMSC-DTL algorithm outperformed that of the t-SVD-MSC algorithm. This was due to the introduction of double tensor mechanism in HRMSC-DTL algorithm which made full use of the intra-view correlation of the original tensor and the inter-

view correlation of the rotated tensor. And hypergraph regularization can effectively preserve the local geometric structure embedded in high-dimensional space. Additionally, it replaced the tensor nuclear norm with the tensor logarithm determinant function in tensor space to better enhance the global low-rank property. To separately study the contribution of these three components in HRMSC-DTL, three tests were conducted.

Specifically, the first test involved replacing the tensor nuclear norm in t-SVD-MSC with the tensor logarithm determinant function. For simplicity, this test was denoted as t-SVD-MSC+w1. In the second test, an additional term for the nuclear norm of the rotated tensor was added to t-SVD-MSC. This test was denoted as t-SVD-MSC+w2. The third test was denoted as t-SVD-MSC+w3, which introduced hypergraph regularization to t-SVD-MSC method. The three tests were conducted on all datasets, and the comparison results in terms of NMI are presented in Table 9. It can be observed that compared to t-SVD-MSC, three tests all showed a certain degree of performance improvement. What's more, the HRMSC-DTL outperformed t-SVD-MSC in all aspects of clustering performance. Therefore, the ablation study demonstrated the necessity of considering the dual tensor mechanism, hypergraph regularization, and the tensor logarithm function in the proposed model.

Table 9 Ablation study: comparison results of HRMSC-DTL and its variants in terms of NMI

Method	Yale	BBCSport	ORL	Notting-Hill	COIL20	Scene15	Wikipedia
t-SVD-MSC	0.908	0.985	0.993	0.900	0.884	0.858	0.480
t-SVD-MSC+w1	0.970	0.989	0.994	0.908	0.953	0.921	0.506
t-SVD-MSC+w2	0.929	1.000	0.996	0.959	0.898	0.867	0.524
t-SVD-MSC+w3	0.845	0.989	**1.000**	0.967	0.960	0.895	0.536
HRMSC-DTL	**1.000**	**1.000**	**1.000**	**0.989**	**0.987**	**0.974**	**0.539**

3.7 Convergence analysis

The convergence of the proposed HRMSC-DTL algorithm was experimentally validated. Fig. 6 displays the convergence curves of the proposed method on the Yale and BBCSport datasets. Based on the algorithmic process described in Section 2.2, the stopping criteria can be divided into four components: $\|\boldsymbol{X}^{(v)}-\boldsymbol{X}^{(v)}\boldsymbol{A}^{(v)}-\boldsymbol{E}^{(v)}\|_{\mathrm{F}}^2$, $\|\boldsymbol{A}^{(v)}-\boldsymbol{P}^{(v)}\|_{\mathrm{F}}^2$, $\|\boldsymbol{A}^{(v)}-\boldsymbol{K}^{(v)}\|_{\mathrm{F}}^2$, and $\|\boldsymbol{A}^{(v)}-\boldsymbol{B}^{(v)}\|_{\mathrm{F}}^2$. The Z-axis in Fig. 6 represents the values of each error term for all views. It can be observed that the HRMSC-DTL algorithm converges to stability around approximately 40 iterations on average.

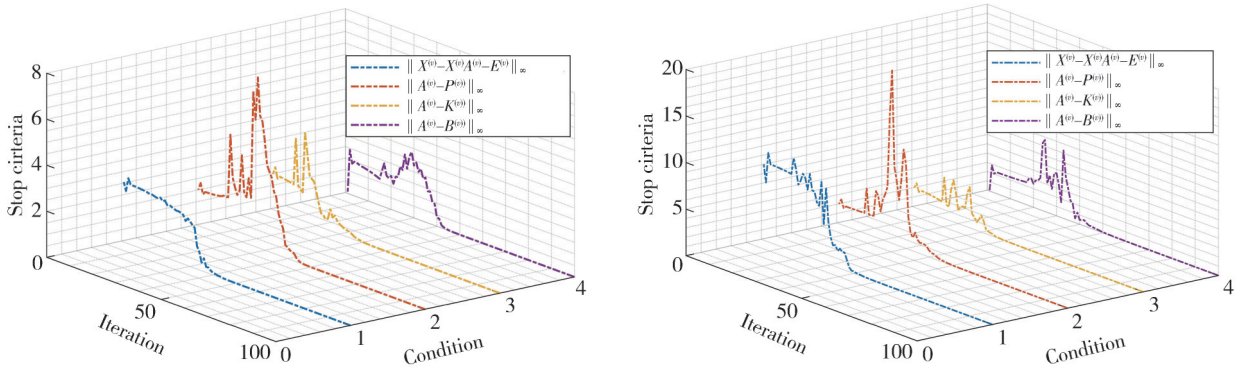

(a) Yale (b) BBCSport

Fig. 6 Stopping criteria and iteration times of HRMSC-DTL method on Yale and BBCSport datasets

4 Conclusions

A hypergraph regularized multi-view subspace clustering model with dual tensor log-determinant was proposed. In this model, replacing the tensor nuclear norm with the non-convex tensor logarithmic determinant function can better improve the global low-rankness of the model. And hypergraph regularization can effectively preserve the local geometric structure embedded in high-dimensional space. Additionally, rotating the original tensor and introducing the dual tensor mechanism effectively utilized the intra view consistency of the original tensor and inter view consistency of the rotated tensor. Finally, an efficient optimization scheme was proposed to handle the non-convex problem effectively. Convergence analysis, parameter sensitivity analysis, and visualization analysis conducted on seven real datasets demonstrated the

advantages of the proposed model in terms of convergence, parameter stability, and accuracy in multi-view clustering tasks.

However, the algorithm's efficiency is relatively low for large-scale datasets. To address this limitation, we will consider implementing anchor sampling algorithms, known for their speed and efficiency. These algorithms select vital landmarks to efficiently represent the entire dataset, reducing computational demands without compromising performance. Future work will focus on integrating these methods to achieve a better balance between clustering performance and computational complexity, thereby enhancing overall performance of the proposed algorithm.

Acknowledgement

This work was supported by National Natural Science Foundation of China (No. 61806006) and Priority Academic Program Development of Jiangsu Higher Education Institutions.

Declaration of conflicting interests

The authors have no conflict of interests related to this publication.

References

[1] MURTAGH F, CONTRERAS P. Algorithms for hierarchical clustering: an overview. WIRES Data Mining and Knowledge Discovery, 2012, 2(1): 86-97.

[2] RAM A, SHARMA A, JALAL A S, et al. An enhanced density based spatial clustering of applications with noise//2009 IEEE International Advance Computing Conference, March 6-7, 2009, Patiala, India. New York: IEEE, 2009: 1475-1478.

[3] YANG J C, ZHAO C. Survey on k-means clustering algorithm. Computer Engineering and Applications, 2019, 55(23): 7-14.

[4] YANG S J, LI L, WANG S H, et al. SkeletonNet: a hybrid network with a skeleton-embedding process for multi-view image representation learning. IEEE Transactions on Multimedia, 2019, 21(11): 2916-2929.

[5] YE Y K, LIU X W, YIN J P, et al. Co-regularized kernel k-means for multi-view clustering//2016 23rd International Conference on Pattern Recognition, December 4-8, 2016, Cancun, Mexico. New York: IEEE, 2016: 1583-1588.

[6] LIU X W, DOU Y, YIN J P, et al. Multiple kernel k-means clustering with matrix-induced regularization//Thirtieth AAAI Conference on Artificial Intelligence, February 12-17, 2016, Phoenix, Arizona, USA. California: AAAI Press, 2016: 1888-1894.

[7] ZHAO Y J, YUN Y, ZHANG X D, et al. Multi-view spectral clustering with adaptive graph learning and tensor schatten p-norm. Neurocomputing, 2022, 468: 257-264.

[8] LI X F, REN Z W, SUN Q S, et al. Auto-weighted tensor schatten p-norm for robust multi-view graph clustering. Pattern Recognition, 2023, 134: 109083.

[9] ZHANG X Q, WANG J, XUE X Q, et al. Confidence level auto-weighting robust multi-view subspace clustering. Neurocomputing, 2022, 475: 38-52.

[10] ZHANG X T, ZHANG X C, LIU H, et al. Multi-task multi-view clustering. IEEE Transactions on Knowledge and Data Engineering, 2016, 28(12): 3324-3338.

[11] CAI B, LU G F, YAO L, et al. High-order manifold regularized multi-view subspace clustering with robust affinity matrices and weighted TNN. Pattern Recognition, 2023, 134: 109067.

[12] YANG Y, WANG H. Multi-view clustering: a survey. Big Data Mining and Analytics, 2018, 1(2): 83-107.

[13] XU C, TAO D C, XU C. A survey on multi-view learning. 2013: 1304.5634. https://arxiv.org/abs/1304.5634v1.

[14] ELHAMIFAR E, VIDAL R. Sparse subspace clustering: algorithm, theory, and applications. IEEE Transactions on Pattern Analysis and Machine Intelligence, 2013, 35(11): 2765-2781.

[15] LIU G C, LIN Z C, YAN S C, et al. Robust recovery of subspace structures by low-rank representation. IEEE Transactions on Pattern Analysis and Machine Intelligence, 2012, 35(1): 171-184.

[16] BRBIĆ M, KOPRIVA I. Multi-view low-rank sparse subspace clustering. Pattern Recognition, 2018, 73: 247-258.

[17] TANG K W, CAO L Y, ZHANG N, et al. Consistent auto-weighted multi-view subspace clustering. Pattern Analysis and Applications, 2022, 25(4): 879-890.

[18] CAO X C, ZHANG C Q, FU H Z, et al. Diversity-induced multi-view subspace clustering//2015 IEEE Conference on Computer Vision and Pattern Recognition, June 7-12, 2015, Boston, MA. New York: IEEE, 2015: 586-594.

[19] ZHANG C Q, FU H Z, LIU S, et al. Low-rank tensor constrained multiview subspace clustering//2015 IEEE International Conference on Computer Vision, December 7-13, 2015, Santiago, Chile. New York: IEEE, 2015: 1582-1590.

[20] WU J L, LIN Z C, ZHA H B. Essential tensor learning for multi-view spectral clustering. IEEE Transactions on Image Processing, 2019, 28(12): 5910-5922.

[21] XIE Y, TAO D C, ZHANG W S, et al. On unifying multi-view self-representations for clustering by tensor multi-rank minimization. International Journal of Computer Vision, 2018, 126(11): 1157-1179.

[22] KILMER M E, BRAMAN K, HAO N, et al. Third-order tensors as operators on matrices: a theoretical and computational framework with applications in imaging. SIAM Journal on Matrix Analysis and Applications, 2013, 34(1): 148-172.

[23] LU C Y, FENG J S, CHEN Y D, et al. Tensor robust principal component analysis: exact recovery of corrupted low-rank tensors via convex optimization//2016 IEEE Conference on Computer Vision and Pattern Recognition, June 27-30, 2016, Las Vegas, NV, USA. New York: IEEE, 2016: 5249-5257.
[24] YIN M, GAO J B, LIN Z C. Laplacian regularized low-rank representation and its applications. IEEE Transactions on Pattern Analysis and Machine Intelligence, 2016, 38(3): 504-517.
[25] KANG Z, PENG C, CHENG Q. Robust subspace clustering *via* smoothed rank approximation. IEEE Signal Processing Letters, 2015, 22(11): 2088-2092.
[26] YANG M, LUO Q L, LI W, et al. Multiview clustering of images with tensor rank minimization via nonconvex approach. SIAM Journal on Imaging Sciences, 2020, 13(4): 2361-2392.
[27] ZHANG Z M, ELY G, AERON S, et al. Novel methods for multilinear data completion and de-noising based on tensor-SVD//2014 IEEE Conference on Computer Vision and Pattern Recognition, June 23-28, 2014, Columbus, OH, USA. New York: IEEE, 2014: 3842-3849.
[28] ZHANG Y, SUN X, CAI H M, et al. Collaborative embedding learning via tensor integration for multi-view clustering. IEEE Transactions on Emerging Topics in Computational Intelligence, 2024, 8(2): 1841-1852.
[29] XIE Y, ZHANG W S, QU Y Y, et al. Hyper-Laplacian regularized multilinear multiview self-representations for clustering and semisupervised learning. IEEE Transactions on Cybernetics, 2020, 50(2): 572-586.
[30] WANG S Q, CHEN Y Y, ZHANG L N, et al. Hyper-Laplacian regularized nonconvex low-rank representation for multi-view subspace clustering. IEEE Transactions on Signal and Information Processing Over Networks, 2022, 8: 376-388.
[31] NG A Y, JORDAN M I, WEISS Y. On spectral clustering: analysis and an algorithm//Advances in Neural Information Processing Systems 14 (NIPS), December 3-8, 2001, Vancouver, British Columbia, Canada. Cambridge, MA: MIT Press, 2001: 849-856.
[32] LIU J Y, LIU X W, YANG Y X, et al. Multiview subspace clustering via co-training robust data representation. IEEE Transactions on Neural Networks and Learning Systems, 2022, 33(10): 5177-5189.
[33] YANG Z Y, XU Q Q, ZHANG W G, et al. Split multiplicative multi-view subspace clustering. IEEE Transactions on Image Processing, 2019, 28(10): 5147-5160.

具有双张量对数行列式的超图正则化多视图子空间聚类

胡克寅[1,2], 李 婷[1,2], 葛洪伟[1,2*]

1. 江南大学 人工智能与计算机学院, 江苏 无锡 214122;
2. 江南大学 康养智能化技术教育部工程研究中心, 江苏 无锡 214122

摘 要: 基于张量奇异值分解的多视图子空间聚类算法, 大多利用张量核范数探索同一样本视图内的相关性, 而忽略了不同视图中样本之间的相关性, 并且没有充分考虑张量核范数作为张量秩函数的凸近似, 平等地对待不同的奇异值会导致张量表示次优。本文提出了一种具有双张量对数行列式的超图正则化多视图子空间聚类算法(HRMSC-DTL)。首先, 通过在每个视图中使用子空间学习来研究一组特定的亲和矩阵, 并引入非凸张量对数行列式函数来替代张量核范数, 以更好地提高全局低秩性。其次, 引入了超拉普拉斯正则化, 以保持嵌入在高维空间中的局部几何结构。此外, 还对原始张量进行旋转, 并引入双张量机制, 以充分利用原始张量的视图内相关性和旋转张量的视图间相关性。同时, 还设计了一种乘子交替方法(ADMM)来求解非凸优化模型。在7个广泛使用的数据集上进行实验, 并与几个主流算法进行比较, 实验结果证明了HRMSC-DTL算法在聚类效果上具有一定的优越性和有效性。

关键词: 多视图聚类; 张量对数行列式函数; 子空间学习; 超图正则化

引用格式: HU Keyin, LI Ting, GE Hongwei. Hypergraph regularized multi-view subspace clustering with dual tensor log-determinant. Journal of Measurement Science and Instrumentation, 2024, 15(4): 466-476.